On Patient-specific models for Accurate SAR Estimations at 7 T

Jin Jin[1], Feng Liu[1], Ewald Weber[1], and Stuart Crozier[1]
[1]*University of Queensland, St Lucia, Queensland, Australia*

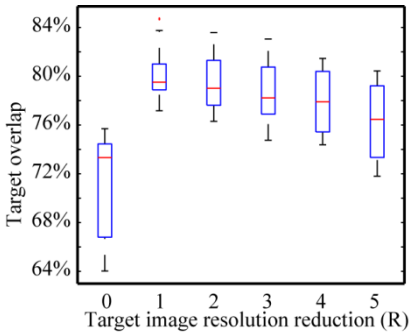

Fig.1 Target overlop at various target image resolutions

INTRODUCTION: Effective prediction and control RF energy absorption, measured as specific absorption rate (SAR), is arguably the most challenging issue for today's high-field MRI applications. Numerical full-wave simulations are typically employed for SAR prediction. However, generic patient models, as commonly used in SAR evaluations, necessitate large safety margins to compensate for inter-subject variations. As a result, the efficiency of RF systems and the quality of the images produced can be non-optimal. To ensure patient safety and to allow confident use of the RF power available in high-field system, we demonstrate an effective approach of creating patient-specific models. Conventionally, the construction of accurate patient models may require full-body high-resolution scans and accurate tissue labelling. Instead, this study creates patient-specific 3D voxel models from existing high quality models using image registration techniques, so that a library of high-resolution 3D images with complete dielectric tissue parameters can be warped to match low-resolution pilot scans of the patient.

$$\theta_{s\to t} = \Psi_t\left(\Psi_s^{-1}\left(\theta_s\right)\right) = \Psi_t \circ \Psi_s^{-1} \circ \theta_s \quad [1]$$

$$TO_{A\to B} = \sum_v \left|\theta_{A,v} \cap \theta_{B,v}\right| \Big/ \sum_v \left|\theta_{B,v}\right| \quad [2]$$

MATERIALS AND METHODS: **I. Models:** Four voxel head models (subject 06, 20, 46 and 51) were arbitrarily chosen from Brainweb (http://www.bic.mni.mcgill.ca/brainweb/). These models were constructed with 11 types of tissues, from segmenting a series of T_1-, T_2-, proton density-weighted MR images, MR angiography (MRA) acquisitions and computed tomography (CT) scans[3]. For more details on the models, please see website. From the corresponding voxel models, the MRI simulator[4] was then employed to simulate 3D T_1-weighted images (also available from Brainweb; spoiled FLASH sequence, *TR* 22 ms, *TE* 9.2 ms, flip angle 30º). These voxel models and simulated images were down-sampled to $2 \times 2 \times 2$ mm^3 resolution for SAR calculations and image registrations, respectively.

II. Registration: A non-rigid registration algorithm DARTEL, short for Diffeomorphic Anatomical Registration using Exponentiated Lie algebra[5], was adopted. In this study, each of the four patient models was used as a resignation target in turn, while the rest of the models were used as registration sources. In this way, 12 registration pairs were created. For each pair of models, DARTEL yielded flow fields (Ψ) that mapped the source image (I_s) and the target images (I_t) to a common template. Ψ_s, for example, denotes the transformation from the common space to the source image space. The tissue distribution of the target can therefore be estimated from that of the source, using Eq.(1), where θ_s is the tissue distribution of the source s; $\theta_{s\to t}$ is the tissue distribution of the target t estimated from the source s; Ψ^{-1} denotes an inverse of the flow field Ψ; and symbol $\circ$ indicates composition. The registration was aided by using a publicly available toolbox SPM8. We also tested the registration method with the target images of variously reduced resolutions, when the original 3D target images were down-sampled retrospectively. Lower resolution target images require less acquisition time and represent faster patient pilot scans.

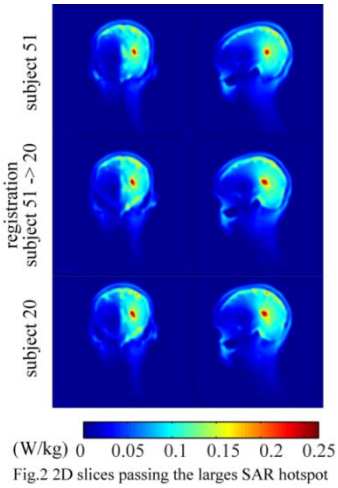

Fig.2 2D slices passing the larges SAR hotspot

III. Voxel model statistical analysis: The target overlap (*TO*) was calculated for each pair of discrete patient models in the form of Eq.(2), where $TO_{A\to B}$ calculates the *TO* agreement between subject *A* and *B*, with respect to the latter's tissue distribution; *v* is the index for each labelled region, such as GM, WM, CSF and so on; $\cap$ denotes intersection; and $|\cdot|$ calculates the number of the voxels in the volume. Essentially, $TO_{A\to B}$ agreement calculates the percentage of the tissue voxels that both *A* and *B* have in common, with respect to the total number of tissue voxels of *B*.

IV. SAR calculations: To calculate SAR for the developed voxel models, electromagnetic (EM) simulations using FDTD method[6] were carried out. A 16-rung high-pass birdcage coil model was employed as EM source (ϕ_{coil} = 30 cm, H_{coil} = 25 cm, ϕ_{shield} = 36 cm, and H_{shield} = 30 cm). The coil was tuned for 7 T applications and was re-tuned whenever the loading condition had changed in the subsequent studies. Circularly polarised excitation was used by exciting at two ports 90° apart. The EM modelling and calculation were performed using commercially available package SEMCAD X (SPEAG, Zurich, Switzerland). The voxel SAR results were scaled to a total input power of 1 W, equally distributed to both ports. The 1-gram SAR was approximated by averaging the voxel SAR values within a $5 \times 5 \times 5$ window. The head models were padded with the neck and shoulder of the NORMAN[7] model (2 mm resolution, and 41 tissue types) to create correct loading.

RESULTS: At each reduction factor R, *TO* measures were performed over 12 pairs of registrations. The results were organised in the box plot, as shown in Fig.1. R = 0 indicates the *TO* measures between the source and original target without registration. It is observed that the registration can significantly improve the *TO* measures at all reduction factors (R = 1 to 5). Also, higher resolution target images (lower *R*) contributed to higher average *TO* with more consistency. The median (red bar across the box) and deviation (approximated by the height of the box) of the *TO* measures degraded gradually and steadily as lower resolution target images were adopted in the registration.

Including the absorbing boundaries, approximately 13.6 million cells were used to resolve the calculation space of the coil-patient models. When different subjects were loaded, adjustments were made whenever necessary to re-tune the coil to 298 MHz. The magnitude and phase of the transmit magnetic fields of different subjects remained largely unchanged among different models (omitted). However, the SAR levels and distributions changed dramatically. Table.1 summarises the maximum 1-gram SAR values and corresponding locations of each original model. Among the four models tested, the largest 1-gram SAR varied by ~16%, and the largest distance between SAR hotspots was as large as 12.1 cm. The results suggested that, using a random model for patient SAR prediction could lead to very large errors.

Table.1 Maximum SAR values and positions

	Max 1g SAR (W/Kg)	[x, y, z] (cm)
subject 06	0.2928	[2.1, 3.0, -0.5]
subject 20	0.2659	[2.4, 3.4, -0.9]
subject 46	0.2678	[-3.2, -7.3, 0.1]
subject 51	0.2532	[3.0, 4.1, -1.3]
registration (51→20)	0.2624	[2.4, 3.4, -0.9]

However, similar SAR values and hotspot locations (1 cm apart) between subject 51 and subject 20 (Table.1) indicated that, if the matching model for a patient was used, SAR values can be predicted within a reasonable range. When examined carefully, subject pair 20-51 had very similar *TO* values in both directions (i.e. $TO_{51\to 20}$ = 75.28% and $TO_{20\to 51}$ = 73.30%), denoting that high mutual target overlap (*MTO*) is a indicator for a pair of matching models. High *MTO* measures not only suggest high tissue conformity in the voxel scale, but also indicate that the two models have similar numbers of total voxel counts and, therefore, similar overall sizes and weights. The intensity and position of the largest SAR hotspot of the estimated model of subject 20, from registering subject 51 to 20, is shown in Table.1 bottom. Here, the resolution of the target image was reduced by a factor of three (*R* = 3), equivalent to using ($1/3^3$ = 3.7%) of the total image data. The maximum 1-gram SAR of the estimated model is very close to that of the target model (subject 20). More remarkably, the location of the hotspot of the registered model coincided exactly with that of the target (subject 20). The results indicated that *MTO* is a viable candidate to evaluate the similarities among subject voxel distributions for the purpose of SAR calculations at 7T. Other registered models were also tested in SAR calculation with varied improvements in prediction accuracy, revealing the importance of having a good matching source for the registration.

CONCLUSION: This proof-of-concept study demonstrates that a patient-specific voxel model for accurate SAR prediction can be created by registering high resolution database images to low resolution pilot scans of the patient, provided that the database and the target patient satisfy high *MTO* condition. The FDTD-based SAR calculation indicates that a patient's maximum 1-gram SAR value and its location can be predicted with remarkable accuracy. Future studies will focus on the development of a dedicated patient database and the improvement of the efficiency and effectiveness of the method.

1.FDA, 1988. 2.IEC, 2002. 3.Aubert-Broche et al, *Neuroimage.* 2006;32(1):138-145. 4. Kwan et al, *IEEE Trans.*, 1999;18(11):1085-1097. 5. Ashburner, *Neuroimage.* 2007;38(1):95-113. 6. Yee, *IEEE Trans.*, 1966;14(3):302-307. 7. Dimbylow, *Phys. Med. Biol.* 1997;42(3):479.